The Astrophysical Journal Letters, 881:L17 (7pp), 2019 August 10 https://doi.org/10.3847/2041-8213/ab32f0

Awakening of the Fast-spinning Accreting Be/X-Ray Pulsar A0538–66*

Lorenzo Ducci[1], Sandro Mereghetti[2], and Andrea Santangelo[1]
[1] Institut für Astronomie und Astrophysik, Kepler Center for Astro and Particle Physics, Eberhard Karls Universität, Sand 1, D-72076 Tübingen, Germany
ducci@astro.uni-tuebingen.de
[2] INAF—Istituto di Astrofisica Spaziale e Fisica Cosmica, Via A. Corti 12, I-20133 Milano, Italy
Received 2019 June 23; revised 2019 July 15; accepted 2019 July 17; published 2019 August 9

Abstract

A0538−66 is a Be/X-ray binary (Be/XRB) hosting a 69 ms pulsar It emitted bright X-ray outbursts with peak luminosity up to $\sim 10^{39}$ erg s^{-1} during the first years after its discovery in 1977. Since then, it was always seen in quiescence or during outbursts with $L_x \lesssim 4 \times 10^{37}$ erg s^{-1}. In 2018 we carried out *XMM-Newton* observations of A0538−66 during three consecutive orbits when the pulsar was close to periastron. In the first two observations we discovered a remarkable variability, with flares of typical durations between ∼2 and 50 s and peak luminosities up to $\sim 4 \times 10^{38}$ erg s^{-1} (0.2–10 keV). Between the flares the luminosity was $\sim 2 \times 10^{35}$ erg s^{-1}. The flares were absent in the third observation, during which A0538−66 had a steady luminosity of 2×10^{34} erg s^{-1}. In all observations, the X-ray spectra consist of a softer component, well described by an absorbed power law with photon index $\Gamma_1 \approx 2$–4 and $N_H \approx 10^{21}$ cm^{-2}, plus a harder power-law component ($\Gamma_2 \approx 0$–0.5) dominating above ∼2 keV. The softer component shows larger flux variations than the harder one, and a moderate hardening correlated with the luminosity. The fast flaring activity seen in these observations was never observed before in A0538−66, nor, to the best of our knowledge, in other Be/XRBs. We explore the possibility that during our observations the source was accreting in a regime of nearly spherically symmetric inflow. In this case, an atmosphere can form around the neutron star magnetosphere and the observed variability can be explained by transitions between the accretion and supersonic propeller regimes.

Key words: accretion, accretion disks – stars: neutron – X-rays: binaries

1. Introduction

Be/X-ray binaries (Be/XRBs) consist of a Be star and, usually, a neutron star (NS). Most of them show a weak persistent X-ray emission ($L_X \lesssim 10^{34}$ erg s^{-1}), interrupted by outbursts ($L_X \lesssim 10^{38}$ erg s^{-1}) that last several weeks. The outbursts are caused by accretion onto the NS of the plasma captured from the circumstellar disks that characterize Be stars (for a review see, e.g., Reig 2011).

A0538−66 is a Be/XRB located in the Large Magellanic Cloud (LMC). It hosts one of the fastest spinning pulsars (period $P = 69$ ms) and has one of the shortest orbital periods ($P_{orb} = 16.6409 \pm 0.0003$ day) and highest eccentricities ($e = 0.72$) among Be/XRBs (White & Carpenter 1978; Rajoelimanana et al. 2017). These characteristics might be at the basis of the peculiar properties observed in this system, both in X-rays and in the optical band.[3] The outbursts observed in the first years after its discovery exceeded the isotropic Eddington limit, reaching peak X-ray luminosities of $L_x \gtrsim 8 \times 10^{38}$ erg s^{-1} (White & Carpenter 1978; Johnston et al. 1979, 1980; Skinner et al. 1980, 1982; Ponman et al. 1984), while all the subsequent observations caught A0538−66 at lower X-ray luminosities, in the range $L_x \approx 5 \times 10^{33}$–$4 \times 10^{37}$ erg s^{-1} (Mavromatakis & Haberl 1993; Campana 1997; Corbet et al. 1997; Campana et al. 2002; Kretschmar et al. 2004).

Remarkably, the pulsations at 69 ms were detected only once, during a bright outburst ($L_x \approx 8 \times 10^{38}$ erg s^{-1}; Skinner et al. 1982) observed by the *Einstein* satellite in 1980. They were never detected in all the subsequent observations, either in quiescence ($L_x \lesssim 10^{34}$ erg s^{-1}) or in outbursts that reached lower luminosities ($L_x \lesssim 10^{38}$ erg s^{-1}). This led to the suggestion that the accreting plasma could overcome the centrifugal magnetospheric barrier and reach the NS surface, thus producing X-ray pulsations, only during episodes of very high accretion rate (Campana et al. 1995; Corbet et al. 1997).

In fact, if the rate of mass gravitationally captured by an NS is below a minimum value that depends on the magnetic field strength and the spin period of the pulsar, the NS magnetosphere is larger than the corotation radius $r_{co} = [GM_{ns} P^2/(4\pi^2)]^{1/3}$ (the distance at which a test particle in a Keplerian orbit corotates with an NS of mass M_{ns} and spin period P). When this occurs, the matter flow is halted at the magnetospheric radius r_m, and assuming that all the potential energy of the mass inflow is converted to radiation, the X-ray luminosity is reduced by a factor r_m/R_{ns}, where R_{ns} is the NS radius. Based on these considerations, Skinner et al. (1982) and Campana et al. (1995) estimated for A0538−66 an upper limit for the magnetic dipole moment of $\mu \lesssim 10^{29}$ G cm^3.

In this Letter we report the results of new *XMM-Newton* observations showing a remarkable variability on short timescales, never observed before in A0538−66 and in other Be/XRBs. Such renewed X-ray activity from A0538−66 possibly preludes to a reactivation of the super-Eddington regime that characterized this source during the first years after its discovery.

2. Observations and Data Analysis

We observed A0538−66 with *XMM-Newton* during three consecutive orbits in 2018. The observations were done at orbital phases close to periastron (see Table 1). Data collected by the European Photon Imaging Camera (EPIC) were

* Based on observations obtained with *XMM-Newton*, an ESA science mission with instruments and contributions directly funded by ESA Member States and NASA.

[3] For the peculiar optical properties shown by A0538−66, see Ducci et al. (2019, 2016) and references therein.

Table 1
Summary of the *XMM-Newton* Observations

Name	Start Time (UTC)	Net Exposure Time (ks)	$\phi_{\rm start}$ [a]	$\phi_{\rm stop}$ [a]
Obs. A	2018 May 15 06:04:50	9.9	−0.0039	0.0091
Obs. B	2018 May 31 22:04:38	12.0	−0.0026	0.0077
Obs. C	2018 Jun 17 12:34:10	12.5	−0.0047	0.0053

Note.
[a] Orbital phase based on the ephemeris of Rajoelimanana et al. (2017). The phase zero of these ephemeris precedes the periastron by $\Delta\phi = 0.038$.

analyzed with the standard Science Analysis System (SAS), version 17.0.0. Observation data files (ODFs) were processed to produce calibrated event lists for pn, MOS1, and MOS2, using the `epproc` and `emproc` tasks. For the pn, single- and double-pixel events (PATTERN $\leqslant$ 4) were used, while for the MOS data, single- to quadruple-pixel events (PATTERN $\leqslant$ 12) were used. Time intervals affected by high background were identified and excluded,[4] resulting in the net exposure times indicated in Table 1. Source events were extracted from a circular region centered at the J2000 coordinates R.A. = 05:35:41.3, decl. = −66:51:51, with an "optimal" extraction radius of 27″ for obs. A and 29″ for obs. B. These radii were calculated with the SAS task `eregionanalyse` to have the maximum signal-to-noise ratio. During obs. C, A0538−66 had a much smaller flux than in obs. A and B, but it was still detected with high significance (detection likelihood $L = 47.69$, corresponding to spurious probability $p \approx 2 \times 10^{-21}$; see Ducci et al. 2013 for the source detection procedure adopted here). For this observation, we used a source extraction radius of 20″. The background was extracted from source-free circular regions. The times of the events were corrected to the solar system barycenter with the `barycen` task.

For each observation, we extracted pn light curves with a bin size of 1 s, background subtracted, and corrected for vignetting, bad pixels, point-spread function (PSF) variations, and quantum efficiency, using the SAS task `epiclccorr`. A0538−66 showed a strong flux variability (see Section 3) and it was affected by pileup during the high-luminosity states. For the pn, we generated a response file that includes pileup corrections.[5] We verified the goodness of the resulting spectrum by comparing it with that obtained using the standard response file and excising the core of the PSF. Since a response file including pileup corrections cannot be produced for the MOS, pileup effects from these data can be removed only by excising the core of the PSF, which leads to a substantial reduction of the statistics. Therefore, in the following analysis we considered only the pn data for the high and intermediate luminosity levels, while we merged pn and MOS data for the low luminosity level (see Section 3 for the definition of the luminosity levels).

Timing and spectral analyses were performed using the standard tools available within HEASOFT v. 6.24 including `xspec` (v. 12.10.0c; Arnaud 1996). For the interstellar absorption, we used the `tbvarabs` model with the Wilms et al. (2000) abundances and the photoionization cross-sections of Verner et al. (1996). A0538−66 is located in the LMC, an environment with a very different metallicity compared to the interstellar medium (ISM) of the Galaxy (Russell & Dopita 1992; Zhukovska & Henning 2013). Therefore, we set the following abundances (with respect to the ISM): O: 0.33; Ne: 0.41; Na: 0.45; Mg: 0.48; Si: 0.59; S: 0.48; Fe: 0.38 (Hughes et al. 1998; Andrievsky et al. 2001). For the other elements heavier than oxygen, we assumed relative abundances of 0.4, and we left the default values for the other parameters. We also noted that the simplest model `tbfeo` gives acceptable results, though with χ^2 values slightly worse than those obtained with `tbvarabs`.

In the following we assume for A0538−66 a distance of $d = 50$ kpc (Alves 2004).

3. Results

The X-ray light curves (1 s bin) of A0538−66 obtained in the three observations are shown in Figure 1. During the first two observations (A, B) the source was in a very peculiar state of rapid variability, characterized by very short flares spanning more than three orders of magnitude, from $F_{\rm min\ A,\ B} \approx 5.7 \times 10^{-13}$ erg cm^{-2} s^{-1} to $F_{\rm max\ A,\ B} \approx 1.4 \times 10^{-9}$ erg cm^{-2} s^{-1} (0.2–12 keV). These fluxes correspond to luminosities of $L_{\rm min\ A,\ B} \approx 1.7 \times 10^{35}$ erg s^{-1} and $L_{\rm max\ A,\ B} \approx 4.2 \times 10^{38}$ erg s^{-1}. The distribution of flare durations shows the presence of a large number of flares shorter than a few seconds (see Figure 1). During observation C, the source flux was stable and much lower than in the previous two observations: $F_{\rm C} \approx 7 \times 10^{-14}$ erg cm^{-2} s^{-1} (0.2–12 keV), which corresponds to $L_{\rm C} \approx 2.1 \times 10^{34}$ erg s^{-1}. Note that the average luminosity during the "nonflaring" time intervals of observations A and B was about eight times higher than $L_{\rm C}$.

We searched for periodic modulations in the 0.2–12 keV pn events using a Rayleigh test Z^2 (e.g., Buccheri et al. 1983). The search was limited to periods longer than 12 ms by the time resolution of the pn camera in small-window mode. No statistically significant pulsations were detected. We calculated the 3σ upper limit on the pulsed fraction $p_{\rm f}$ (defined as the ratio between the difference and sum of the maximum and minimum count rates of the pulse profile) using the method described in Brazier (1994), in the period range ∼50–100 ms (including the value of ∼69 ms discovered by Skinner et al. 1982). We found the following: obs. A: $p_{\rm f} \leqslant 15\%$; obs. B: $p_{\rm f} \leqslant 9\%$; obs. C: $p_{\rm f} \leqslant 76\%$. The pulsed fraction of A0538−66 measured by Skinner et al. (1982) for the unique detection of pulsation from this source was ∼26%.

To search for possible spectral variability as a function of the X-ray luminosity we divided the data in three subsets based on the values of the pn count rate: low (rate <5 c s^{-1}), intermediate (5 $\leqslant$ rate $\leqslant$ 80 c s^{-1}), and high (rate >80 c s^{-1}). The boundary between the intermediate and high level was chosen to have approximately the same statistics in both data sets. After checking that the pn and MOS spectra for the low state gave consistent results, we combined them using the SAS task `epicspeccombine`. We used a similar procedure to combine the pn spectra of observations A and B for the intermediate and high levels.

We fitted these spectra in the 0.2–12 keV energy range. Using simple single-component models we could not obtain good fits because the spectra clearly show two distinct components in the soft ($\lesssim$2 keV) and hard energy ranges. In the following, we concentrate on the simplest phenomenological model that gave a

[4] See the *XMM-Newton* thread: https://www.cosmos.esa.int/web/xmm-newton/sas-thread-epic-filterbackground.
[5] We followed the procedure described in the SAS thread: https://www.cosmos.esa.int/web/xmm-newton/sas-thread-epatplot.

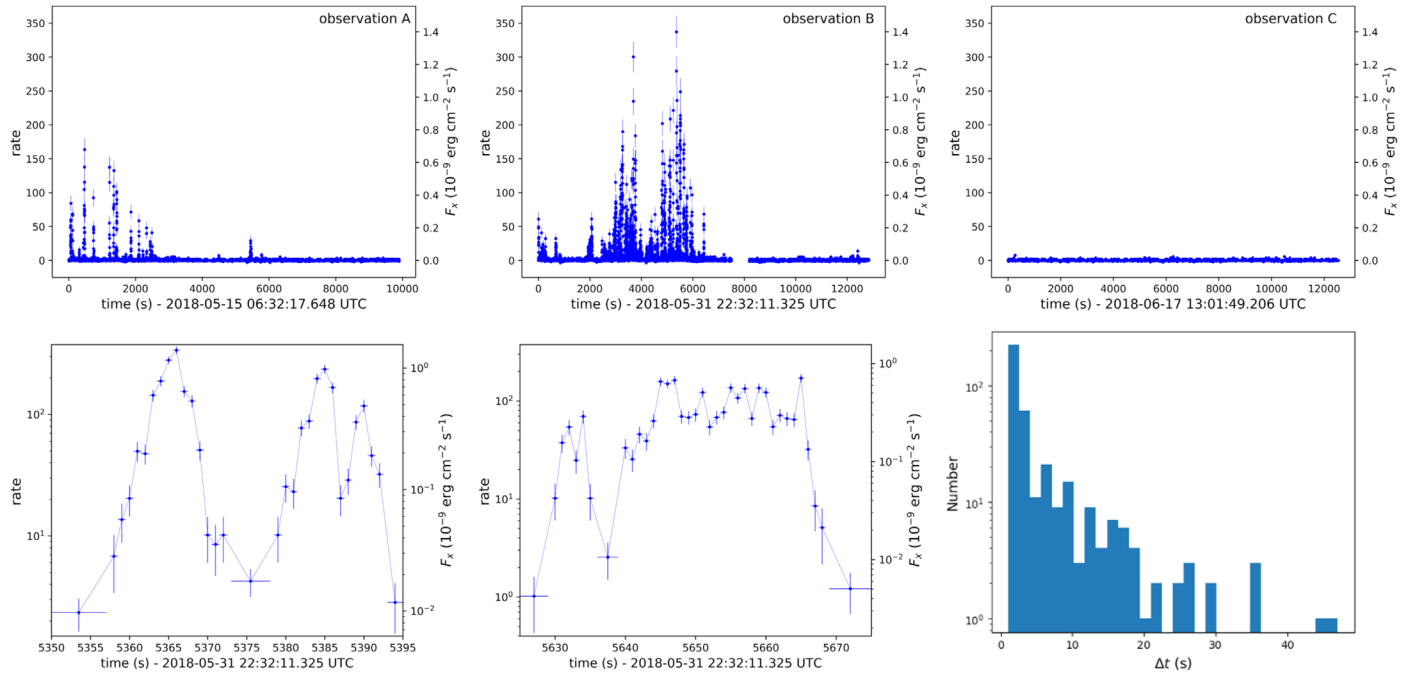

Figure 1. Top panel: pn light curves (0.2–12 keV, bin time 1 s) of A0538−66 during the three observations. Bottom left and bottom middle panels: two zoomed in sections of the light curve of observation B, rebinned at low rates, to better show the structures of the flares. Bottom right panel: distribution of the durations of the flares (Δt).

reasonably good fit, i.e., the sum of two absorbed power laws (with the addition of a broad line at ∼6.4 keV in the high- and intermediate-level spectra).

The best-fit parameters are reported in Table 2, and the corresponding spectra and residuals are shown in Figure 2. Since the column density is similar in the three spectra, we also tried to fit them fixing $N_{\rm H}$ to a common value. This led to similar best-fit parameters for the power laws, but with worse chi-squared values.

The comparison of the best-fit parameters for the three states indicates a moderate spectral variability as a function of luminosity. In particular, between the intermediate and high level, the flux of the softer component increases by a larger factor (∼6) than that of the harder one (∼3). At the same time, the low-energy power law becomes harder.

The intermediate- and high-level spectra show a broad emission feature with energy consistent with the $K\alpha$ emission at 6.4 keV from Fe XXIII. We tried to fit this feature with reflection disk models like `diskline`, but this resulted in worse fits than those obtained with a Gaussian profile.

Table 2
Best-fit Spectral Parameters of the Absorbed Two-component Power Law plus a Gaussian Model to Describe the Three Luminosity States of A0538−66 (Errors at 1σ Confidence Level)

Parameters[a]	Low	Intermediate	High
$N_{\rm H}$ (10^{22} cm^{-2})	$0.13^{+0.09}_{-0.07}$	0.119 ± 0.006	$0.098^{+0.007}_{-0.007}$
Γ_1	$2.4^{+0.7}_{-0.6}$	4.0 ± 0.1	$3.04^{+0.10}_{-0.09}$
Flux$_1$	$0.054^{+0.016}_{-0.009}$	$43.3^{+2.3}_{-2.0}$	$272.8^{+7.4}_{-6.9}$
Γ_2	$-0.04^{+0.26}_{-0.35}$	0.54 ± 0.05	0.49 ± 0.16
Flux$_2$	$0.21^{+0.02}_{-0.03}$	$46.8^{+1.8}_{-1.9}$	$143.6^{+10.2}_{-10.6}$
$E_{\rm line}$ (keV)	–	6.12 ± 0.11	$6.45^{+0.16}_{-0.15}$
σ (keV)	–	$1.02^{+0.19}_{-0.17}$	0.65 ± 0.13
norm line	–	$9.3^{+1.8}_{-1.5} \times 10^{-4}$	$2.00^{+0.49}_{-0.46} \times 10^{-3}$
χ^2 (d.o.f.)	1.107 (39)	1.0944 (376)	1.2166 (259)
norm$_2$/norm$_1$	$3.89^{+0.31}_{-0.22}$	$1.08^{+0.07}_{-0.06}$	0.52 ± 0.08

Notes. Unabsorbed fluxes in units of 10^{-12} erg cm^{-2} s^{-1} (0.3−10 keV).
[a] Model tbvarabs*(pegpwrlw+pegpwrlw+gaus) in XSPEC.

4. Discussion

The flaring variability detected in observations A and B, characterized by flux changes as large as three orders of magnitude on timescales of a few seconds was never observed before in A0538−66, nor in other Be/XRBs. Flaring activity has been observed in a few other high-mass X-ray binaries (HMXBs), but with less extreme properties. For example, the Be/XRB A0535 + 26 showed X-ray flares preceding an outburst in 2005 September (Caballero et al. 2008), but they were much longer ($\Delta t \approx 10^4$ s), fainter (peak X-ray luminosity of 5×10^{36} erg s^{-1}), and with a smaller dynamic range ($\Delta L \lesssim 10$). Postnov et al. (2008) explained them as the result of an interchange instability that develops in the boundary layer between the accretion disk and the NS magnetosphere during the transition from the propeller to the accretion state. Similar flares were also observed in another Be/XRB, EXO 2030 + 375, and explained with an accretion disk–magnetospheric instability, leading to a cyclic increase of the mass accretion rate on the viscous timescale at the magnetosphere (Spruit & Taam 1993; Klochkov et al. 2011).

Strong and rapid variability is also present in the supergiant fast X-ray transients (SFXTs), a subclass of HMXBs with OB

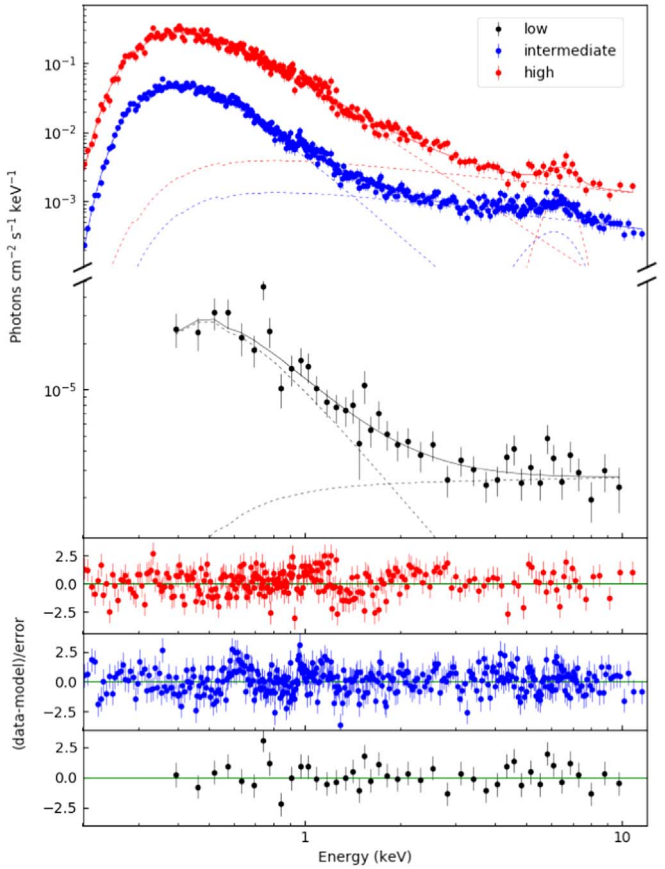

Figure 2. *XMM-Newton* spectra of A0538−66 during the three luminosity levels, fitted with two absorbed power laws (plus a Gaussian line for the intermediate and high luminosity levels). The lower panels show the residuals of the fits.

supergiant mass donors (see, e.g., Sidoli 2013; Romano 2015). Their flares have typical peak luminosity of 10^{36}–10^{37} erg s^{-1} (thus, 10−100 times fainter than those of A0538−66) and durations of $\sim 10^2$–10^3 s. The mechanism responsible for the flares in SFXTs is not yet clear, although many models involving wind variability, gating mechanisms and settling accretion regimes have been proposed (e.g., Zand 2005; Grebenev & Sunyaev 2007; Bozzo et al. 2008; Ducci et al. 2009, 2010; Shakura et al. 2014).

The flares we observed in A0538−66 are more reminiscent of those seen in some accreting millisecond X-ray pulsars (AMXPs; Patruno et al. 2009; Patruno & D'Angelo 2013; Ferrigno et al. 2014). As in some of the models quoted above for other sources, the AMXPs flares also were explained in terms of magnetic gating mechanisms that can occur in disk-accreting sources when $r_{\rm m} \approx r_{\rm co}$ (e.g., Spruit & Taam 1993; D'Angelo & Spruit 2010). Notably, the AMXPs flares also have lower peak luminosities ($\lesssim 10^{36}$ erg s^{-1}) and a smaller dynamical range ($\Delta L \approx$ 10–50) than those observed in A0538−66. Another X-ray binary showing similar flares is GRO J1744−28, also known as the "Bursting Pulsar." It consists of a neutron star with spin period of ∼0.467 s accreting from a low-mass companion star. It emits type II bursts, likely caused by viscous instabilities in the accretion disk (see, e.g., Bagnoli et al. 2015 and references therein). These bursts have a duration of the order of a few seconds and can reach peak luminosities of $\approx 10^{40}$ erg s^{-1}, but the amplitude of variability

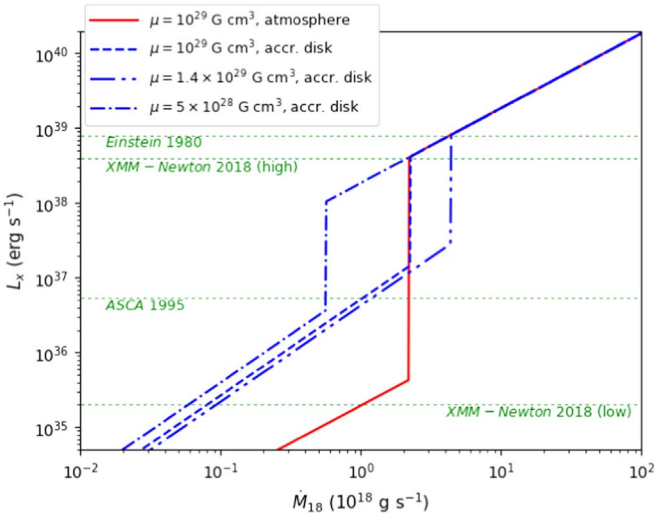

Figure 3. Expected luminosity of A0538−66 as a function of the mass captured rate. Blue dashed, dotted–dashed, and dotted–dotted–dashed lines show the case of centrifugal inhibition of accretion with an accretion disk, as proposed to explain the previous outbursts of A0538−66, for different values of μ. The red solid line shows the luminosity regimes for the spherically symmetric accretion scenario of DP81. Horizontal green dotted lines show the average X-ray luminosities of the most relevant outbursts displayed by A0538−66 (*Einstein* 1980: Skinner et al. 1982; *ASCA* 1995: Corbet et al. 1997).

with respect to the nonbursting luminosity is of $\Delta L_{\rm x} \approx$ 6–40 (Giles et al. 1996; Sazonov et al. 1997; Court et al. 2018).

As mentioned above, Campana et al. (1995) noticed that the presence of pulsations during the 1980 super-Eddington flare of A0538−66 implies an upper limit on its magnetic dipole $\mu \lesssim 10^{29}$ G cm^3. They also pointed out that the fainter outbursts ($L_{\rm x} \approx 5 \times 10^{36}$–$4 \times 10^{37}$ erg s^{-1}) seen with *ROSAT* and *ASCA* could be explained with accretion onto the magnetosphere and that the soft *ROSAT* spectra of the low-luminosity states are in agreement with the expected temperature calculated by Stella et al. (1994) for a standard accretion disk truncated at $r_{\rm m}$. In this case, assuming that all the potential energy of the accretion flow is released at the magnetosphere and converted to X-ray radiation, a luminosity of $L_{\rm m} \approx GM_{\rm ns}\dot{M}_{\rm c}/r_{\rm m}$ is produced (see also King & Cominsky 1994; Stella et al. 1994). Given the short spin period of A0538−66, a luminosity jump of a factor ∼30 (independent of the value of μ) is expected when $r_{\rm m}$ overcomes $r_{\rm co}$ as a result of a decrease of the inflowing mass rate (Corbet et al. 1997). This is illustrated in Figure 3, where the transitions between the two accretion regimes for different values of μ are compared to the X-ray luminosities of the most relevant X-ray observations of A0538−66. Clearly, the luminosity variations seen in the *XMM-Newton* observations reported here are too large to be explained with this scenario.

In the following, we explore the possibility that during our observation A0538−66 was in a regime of spherical accretion and its variability was caused by rapid changes between the different accretion regimes discussed in Davies & Pringle (1981, hereafter DP81).

An accretion disk can form only if the specific angular momentum of the gravitationally captured matter is sufficiently large. This can be checked by considering the circularization radius (see, e.g., Frank et al. 2002), which in case of wind accretion can be estimated as

$$r_{\rm circ} = \xi G^3 M_{\rm ns}^3 \omega^2 v_{\rm rel}^{-8}, \quad (1)$$

where G is the gravitational constant, ω is the orbital angular velocity, $M_{\rm ns}$ is the NS mass,[6] and $v_{\rm rel}$ is the relative velocity between the NS and the wind.[7] The factor $\xi \sim 0.2$ accounts for the reduction in angular momentum due to inhomogeneities in the wind (Ikhsanov et al. 2001). Due to the highly eccentric orbit with a large inclination with respect to the equatorial plane of the Be star (Rajoelimanana et al. 2017), for most of the time the NS is embedded in the fast ($v \gtrsim 500\,{\rm km\,s^{-1}}$) and weak polar wind of the companion star. Therefore, $r_{\rm circ} \approx 2 \times 10^6$ cm, much smaller than the magnetospheric radius ($\gtrsim 10^8$ cm), and a disk cannot form. A transient accretion disk might form when the NS crosses the Be circumstellar disk, where the wind is denser and slower, but this possibility also is uncertain. For a wind velocity law $v_{\rm w}(r) = v_0 (r/R_{\rm d})^{n-2}$, with $v_0 = 5$–$50\,{\rm km\,s^{-1}}$, $2.5 \leqslant n \leqslant 4$ (Waters et al. 1989), and $R_{\rm d} = 10\,R_\odot$, we estimate $v_{\rm rel}$ at periastron in the range $\sim 3.1-4.8 \times 10^7$ cm. By comparing the resulting $r_{\rm circ} \approx 0.13$–$4.1 \times 10^8$ cm with the values of $r_{\rm m} \approx 1.1 \times 10^8$ cm discussed below, it can be seen that there are regions in the parameter space for which a disk cannot form. Finally, we note that the transient nature of an accretion disk or its absence is also supported by the occasional lack of the He II λ4686 emission line at times of outbursts (McGowan & Charles 2003). Based on these considerations, we believe that our assumption of (nearly) spherical accretion is not unreasonable and we can apply the framework described by DP81.

From the peak luminosity of the flares we can estimate the rate of "captured" mass, $\dot{M}_{\rm c} \approx 2 \times 10^{18}\,{\rm g\,s^{-1}}$. If the drops in luminosity between the flares are caused by the sudden activation of the magnetic barrier, the magnetospheric radius must be close to the corotation radius $r_{\rm co} = 2.8 \times 10^7$ cm. Therefore, using the canonical definition of $r_{\rm m}$ (see Equation (2.5) in DP81),

$$r_{\rm m} \approx 3.6 \times 10^7 \dot{M}_{18}^{-2/7} \mu_{29}^{4/7} M_{1.4}^{-1/7}\ {\rm cm}\ , \qquad (2)$$

where $\mu_{29} = \mu/(10^{29}\ {\rm G\,cm^3})$ and $\dot{M}_{18} = \dot{M}_{\rm c}/(10^{18}\ {\rm g\,s^{-1}})$, setting $\dot{M}_{18} = 2$, we find that there is a transition from accretion to inhibition of accretion when $\mu_{29} \approx 1$.[8]

DP81 showed that, under certain conditions, a quasi-static atmosphere can form around the NS magnetosphere. The atmosphere is heated by the conversion of rotational energy of the spinning-down NS, that is transported from the base of the atmosphere outward, through convective and turbulent motions. The atmosphere remains stable if it does not cool down significantly by radiative losses. When the magnetospheric radius overcomes the corotation radius, the supersonic propeller regime activates. DP81 showed that in this case an atmosphere with an effective polytropic index of $n = 1/2$ forms around the NS. Its lower boundary (the magnetospheric radius) moves to

$$r_{\rm m,sup} \approx 8 \times 10^7 \mu_{29}^{4/9} \dot{M}_{18}^{-2/9} v_8^{-4/9} M_{1.4}^{1/9}\ {\rm cm}, \qquad (3)$$

where $v_8 = v_{\rm rel}/(10^8\,{\rm cm\,s^{-1}}) \approx 0.35$ for A0538−66. Setting $\dot{M}_{18} = 2$ in Equation (3), we get $r_{\rm m,sup} \approx 1.1 \times 10^8$ cm. $r_{\rm m,sup}$ is larger than the magnetospheric radius given by Equation (2). Lipunov (1987) showed that this can be qualitatively explained by the decrease in density and pressure of the atmosphere due to its heating, which causes its expansion. DP81, and later Ikhsanov (2002), showed that the atmosphere in the supersonic propeller regime is stable against bremsstrahlung cooling and does not collapse until the mass captured rate is lower than

$$\dot{M}_{\rm lim} \approx 3.1 \times 10^{18} M_{1.4} v_8\ {\rm g\,s^{-1}}. \qquad (4)$$

The exact value of $\dot{M}_{\rm lim}$ is subject to some uncertainties (Bozzo et al. 2008). It is important to note that $\dot{M}_{\rm lim}$ is derived from the mixing length theory of convection, which is a crude simplification of the physical process of convection (Cox & Giuli 1968). $\dot{M}_{\rm lim}$ also depends on the detailed derivation presented in different works. If we use the treatment of the convective efficiency parameter of Kippenhahn & Weigert (1990; instead of that of Cox & Giuli 1968 used by Ikhsanov 2002), $\dot{M}_{\rm lim}$ would be higher by a factor of two.

The luminosity in the supersonic propeller regime is produced by the conversion of the rotational energy dissipated at the lower boundary of the atmosphere (DP81), and is given by

$$L_{\rm sd} \approx 8 \times 10^{34} \dot{M}_{18} v_8^2\ {\rm erg\,s^{-1}}. \qquad (5)$$

For $\dot{M}_{18} = 2$ and $v_8 = 0.35$, we obtain $L_{\rm sd} \approx 2 \times 10^{34}\ {\rm erg\,s^{-1}}$, which is lower than the intraflare luminosity in the first two *XMM-Newton* observations. In addition, we did not observe strong spectral variations between the flares and the low-luminosity states, although these could have been expected in the framework of the scenario of DP81 (see also Ikhsanov 2001). These difficulties can be overcome if we consider the possibility that a fraction of the material in contact with the magnetosphere leaks toward the NS surface through the magnetospheric barrier via magnetic reconnections. According to the "reconnection driven accretion model" of Ikhsanov (2001) and the work of Elsner & Lamb (1984), the rate of plasma accreted because of reconnection of the magnetic field lines is

$$\dot{M}_{\rm rec} \approx 10^{15} \left[\frac{\alpha_{\rm R}}{0.1}\right] \left[\frac{\lambda_{\rm m}}{0.01 r_{\rm m}}\right] \dot{M}_{18}\ {\rm g\,s^{-1}}, \qquad (6)$$

where $\alpha_{\rm R} \approx 0.1$ and $\lambda_{\rm m} \approx 0.1$–$0.01 r_{\rm m}$ (Ikhsanov 2001 and references therein). Using Equation (6), we find that the luminosity caused by magnetic reconnections in A0538−66 could be of the order of $L_{\rm x} \approx 10^{35}\ {\rm erg\,s^{-1}}$, in agreement with the observations. The red solid line of Figure 3 shows the expected X-ray luminosity in this scenario, including both the contributions of Equations (5) and (6). The instabilities arising around the transition between accretion and supersonic

[6] We take $M_{\rm ns} = 1.4\,M_\odot$ in the whole Letter.

[7] For the calculation of the orbital separation and the relative wind velocity, we followed Smart (1965), Waters et al. (1989), and Rajoelimanana et al. (2017) for the parameters of the binary system.

[8] We note that for the mass captured rate implied by the X-ray luminosities of the flares, A0538−66 could be in the subsonic regime, with the formation of an adiabatic atmosphere surrounding the magnetosphere when $r_{\rm m} < r_{\rm co}$ (DP81). Although, for the value of $\dot{M}_{\rm c}$ mentioned above the adiabatic atmosphere would be stable against damping of convective motions caused by bremmstrahlung radiative cooling, from Equation (21) in Bozzo et al. (2008) it can be noted that during the subsonic regime the luminosity produced by the matter entering the magnetosphere through Kelvin–Helmholtz instability has the same order of magnitude of the luminosity the pulsar would have if it accreted on its surface. In this case, the effects of the X-ray radiation coming from the NS on the atmosphere may no longer be negligible and this regime of accretion could therefore be absent.

propeller regime might produce the flares of the *XMM-Newton* observations presented here.

Finally, we mention a possible qualitative interpretation of the spectral variability observed in our data. It is based on the possibility that, during the low luminosity levels, accretion is not completely inhibited by the centrifugal barrier and a fraction of the matter can leak from the inner layers of the atmosphere onto the NS surface (see, e.g., Elsner & Lamb 1984). This is supported by the observation of accretion episodes at luminosities below the transition limit between the accretion and the centrifugal inhibition regimes observed in other X-ray binaries (e.g., Rutledge et al. 2007; Doroshenko et al. 2014). In the framework of the idea proposed by Zhang et al. (1998) to explain the hard X-ray spectrum of Aql X−1, the soft spectral component of A0538−66 could be produced by the accretion of matter onto the NS surface. The hard component is produced by inverse Compton scattering of the photons of the soft component by the electrons in the atmosphere just outside the magnetosphere during the flares and the low-luminosity states (if magnetic reconnections takes place). According to the recent findings of Tsygankov et al. (2019), bulk Comptonization of the leaking matter should be negligible because of the small optical depth expected at the accretion rates occurring during the low luminosity level of A0538−66. When the accretion on the surface decreases dramatically, the soft component decreases suddenly. The hard component also decreases as a result of the decrease of the seed photons. However, according to Wang & Robertson (1985), the temperature outside the magnetosphere during the supersonic propeller regime can increase and the power law that describes the hard X-ray emission produced by Comptonization will become harder, similarly to what was observed in A0538−66.

5. Conclusions

Our new X-ray data (obtained 16 years after the last observation of A0538−66) led to the discovery of a peculiar flaring behavior, never seen before in this source. Although other explanations for the observed variability cannot be excluded, we speculate that the strong and rapid flares occur because the source was accreting from a spherically symmetric flow, not mediated by an accretion disk. In these conditions an atmosphere can form above the NS magnetosphere and flares might be produced by rapid changes between the accretion and supersonic propeller regime. On the other hand, the less dramatic variability observed in previous occasions is consistent with episodes of accretion from a disk. Both accretion scenarios are possible provided that the magnetic dipole moment is $\mu \approx 10^{29}$ G cm^3. In general, a thorough study of the spectral properties would require a better coverage at higher energies to better constrain the hard component.

L.D. acknowledges the kind hospitality of INAF/IASF-Milano, where part of this work was carried out. This work is supported by the Bundesministerium für Wirtschaft und Technologie through the Deutsches Zentrum für Luft und Raumfahrt (grant FKZ 50 OG 1602) and by the agreement ASI/INAF I/037/12/0.

ORCID iDs

Lorenzo Ducci https://orcid.org/0000-0002-9989-538X
Sandro Mereghetti https://orcid.org/0000-0003-3259-7801

References

Alves, D. R. 2004, NewAR, 48, 659
Andrievsky, S. M., Kovtyukh, V. V., Korotin, S. A., Spite, M., & Spite, F. 2001, A&A, 367, 605
Arnaud, K. A. 1996, in ASP Conf. Ser. 101, Astronomical Data Analysis Software and Systems V, ed. G. H. Jacoby & J. Barnes (San Francisco, CA: ASP), 17
Bagnoli, T., in't Zand, J. J. M., D'Angelo, C. R., & Galloway, D. K. 2015, MNRAS, 449, 268
Bozzo, E., Falanga, M., & Stella, L. 2008, ApJ, 683, 1031
Brazier, K. T. S. 1994, MNRAS, 268, 709
Buccheri, R., Bennett, K., Bignami, G. F., et al. 1983, A&A, 128, 245
Caballero, I., Santangelo, A., Kretschmar, P., et al. 2008, A&A, 480, L17
Campana, S. 1997, A&A, 320, 840
Campana, S., Stella, L., Israel, G. L., et al. 2002, ApJ, 580, 389
Campana, S., Stella, L., Mereghetti, S., & Colpi, M. 1995, A&A, 297, 385
Corbet, R. H. D., Charles, P. A., Southwell, K. A., & Smale, A. P. 1997, ApJ, 476, 833
Court, J. M. C., Altamirano, D., Albayati, A. C., et al. 2018, MNRAS, 481, 2273
Cox, J. P., & Giuli, R. T. 1968, Principles of Stellar Structure (New York: Gordon & Breach)
D'Angelo, C. R., & Spruit, H. C. 2010, MNRAS, 406, 1208
Davies, R. E., & Pringle, J. E. 1981, MNRAS, 196, 209
Doroshenko, V., Santangelo, A., Doroshenko, R., et al. 2014, A&A, 561, A96
Ducci, L., Covino, S., Doroshenko, V., et al. 2016, A&A, 595, A103
Ducci, L., Mereghetti, S., Hryniewicz, K., Santangelo, A., & Romano, P. 2019, A&A, 624, A9
Ducci, L., Sasaki, M., Haberl, F., & Pietsch, W. 2013, A&A, 553, A7
Ducci, L., Sidoli, L., Mereghetti, S., Paizis, A., & Romano, P. 2009, MNRAS, 398, 2152
Ducci, L., Sidoli, L., & Paizis, A. 2010, MNRAS, 408, 1540
Elsner, R. F., & Lamb, F. K. 1984, ApJ, 278, 326
Ferrigno, C., Bozzo, E., Papitto, A., et al. 2014, A&A, 567, A77
Frank, J., King, A., & Raine, D. J. 2002, Accretion Power in Astrophysics (3rd ed.; Cambridge: Cambridge Univ. Press), 398
Giles, A. B., Swank, J. H., Jahoda, K., et al. 1996, ApJL, 469, L25
Grebenev, S. A., & Sunyaev, R. A. 2007, AstL, 33, 149
Hughes, J. P., Hayashi, I., & Koyama, K. 1998, ApJ, 505, 732
Ikhsanov, N. R. 2001, A&A, 367, 549
Ikhsanov, N. R. 2002, A&A, 381, L61
Ikhsanov, N. R., Larionov, V. M., & Beskrovnaya, N. G. 2001, A&A, 372, 227
in't Zand, J. J. M. 2005, A&A, 441, L1
Johnston, M. D., Bradt, H. V., Doxsey, R. E., et al. 1979, ApJL, 230, L11
Johnston, M. D., Griffiths, R. E., & Ward, M. J. 1980, Natur, 285, 26
King, A., & Cominsky, L. 1994, ApJ, 435, 411
Kippenhahn, R., & Weigert, A. 1990, Stellar Structure and Evolution (Berlin: Springer), 192
Klochkov, D., Ferrigno, C., Santangelo, A., et al. 2011, A&A, 536, L8
Kretschmar, P., Wilms, J., Staubert, R., Kreykenbohm, I., & Heindl, W. A. 2004, in ESA Special Publication 552, 5th INTEGRAL Workshop on the INTEGRAL Universe, ed. V. Schoenfelder, G. Lichti, & C. Winkler, 329
Lipunov, V. M. 1987, The Astrophysics of Neutron Stars (Berlin: Springer)
Mavromatakis, F., & Haberl, F. 1993, A&A, 274, 304
McGowan, K. E., & Charles, P. A. 2003, MNRAS, 339, 748
Patruno, A., & D'Angelo, C. 2013, ApJ, 771, 94
Patruno, A., Watts, A., Klein Wolt, M., Wijnands, R., & van der Klis, M. 2009, ApJ, 707, 1296
Ponman, T. J., Skinner, G. K., & Bedford, D. K. 1984, MNRAS, 207, 621
Postnov, K., Staubert, R., Santangelo, A., et al. 2008, A&A, 480, L21
Rajoelimanana, A. F., Charles, P. A., Meintjes, P. J., et al. 2017, MNRAS, 464, 4133
Reig, P. 2011, Ap&SS, 332, 1
Romano, P. 2015, JHEAp, 7, 126
Russell, S. C., & Dopita, M. A. 1992, ApJ, 384, 508
Rutledge, R. E., Bildsten, L., Brown, E. F., et al. 2007, ApJ, 658, 514
Sazonov, S. Y., Sunyaev, R. A., & Lund, N. 1997, AstL, 23, 286
Shakura, N., Postnov, K., Sidoli, L., & Paizis, A. 2014, MNRAS, 442, 2325
Sidoli, L. 2013, arXiv:1301.7574
Skinner, G. K., Bedford, D. K., Elsner, R. F., et al. 1982, Natur, 297, 568
Skinner, G. K., Shulman, S., Share, G., et al. 1980, ApJ, 240, 619
Smart, W. M. 1965, Text-book on Spherical Astronomy (Cambridge: Cambridge Univ. Press)

Spruit, H. C., & Taam, R. E. 1993, ApJ, 402, 593
Stella, L., Campana, S., Colpi, M., Mereghetti, S., & Tavani, M. 1994, ApJL, 423, L47
Tsygankov, S. S., Rouco Escorial, A., Suleimanov, V. F., et al. 2019, MNRAS, 483, L144
Verner, D. A., Ferland, G. J., Korista, K. T., & Yakovlev, D. G. 1996, ApJ, 465, 487
Wang, Y.-M., & Robertson, J. A. 1985, A&A, 151, 361
Waters, L. B. F. M., de Martino, D., Habets, G. M. H. J., & Taylor, A. R. 1989, A&A, 223, 207
White, N. E., & Carpenter, G. F. 1978, MNRAS, 183, 11P
Wilms, J., Allen, A., & McCray, R. 2000, ApJ, 542, 914
Zhang, S. N., Yu, W., & Zhang, W. 1998, ApJL, 494, L71
Zhukovska, S., & Henning, T. 2013, A&A, 555, A99